

Analytical / Experimental Study of Vibration of a Room-Sized Airspring-Supported Slab

Hal Amick¹, Bea Sennewald², Norman C. Pardue², Clayton Teague³, Brian Scaze³

ABSTRACT

This paper reports the results of the finite element analysis and *in-situ* testing of a large-scale (4m x 10m) pneumatically isolated concrete slab. The slab was constructed as a design prototype for next-generation metrology laboratories at the National Institute of Standards and Technology (NIST) in Gaithersburg, MD. Data include computed and measured modeshapes and natural frequencies, as well as the measured performance under ambient conditions. The slab was able to achieve one-third octave band amplitudes as low as 0.25 $\mu\text{m}/\text{sec}$ (10 $\mu\text{in}/\text{sec}$) over some frequency ranges.

1. INTRODUCTION

Much of the research conducted by the National Institute of Standards and Technology (NIST) requires high levels of accuracy, which necessitates very stable environments and very low levels of vibration. Limiting the transmission of ambient vibration to sensitive experiments has been a long-standing need at NIST. One goal of the ATLs is to provide highly controlled vibration environments in laboratory spaces. Experience at European metrology laboratories suggested that the use of pneumatically supported concrete inertia slabs could permit achievement of this goal. However, in a literature search, very little information regarding actual properties and performance of large isolated slabs was found. NIST commissioned design and construction of a prototype slab of significant size—4 m x 10 m (about 13 ft x 32 ft)—using readily available vibration-isolation components.

This paper presents the results of a thorough study of the modal properties of the prototype slab using experimental methods and finite element modeling. The intent of the study was two-fold: (1) to document the dynamic characteristics of the prototype slab and (2) to determine the extent to which finite element modeling could be used as a design tool to predict slab behavior. A byproduct of the documentation of dynamic characteristics was to be that the scientists who would use the slab for experiments would have a better understanding of how their vibration environments would vary from one location to the next.

2. OVERVIEW OF STUDY

Assessment of Existing NIST Campuses. A thorough vibration evaluation was carried out on two candidate sites at each campus, as well as a vibration survey of much of the existing NIST laboratory space. The sites selected for the ATLs are already relatively quiet, with maximum one-third-octave band rms velocity amplitudes on the order of 3 micrometers/sec ($\mu\text{m}/\text{s}$) or 125 microinches/sec. The frequencies at which the maxima occur are between 10 and 20 Hz.

¹ Colin Gordon & Associates (work performed while at Acentech Incorporated)

² Henningson, Durham & Richardson, Alexandria, VA

³ National Institute of Standards and Technology (NIST), Gaithersburg, MD

Development of Design Criteria. NIST scientists and the ATL design team agreed that an appropriate vibration criterion for the isolated slabs would be a velocity amplitude of $0.75 \mu\text{m/s}$ —one-fourth of the typical on-grade velocity amplitude—at frequencies above the “skirt” of the airspring resonance curve, about 8 Hz. In addition, the design team decided that the fundamental resonance frequency associated with internal deformation of the slab should be somewhat greater than 30 Hz. The selection of these particular values was somewhat arbitrary; the amplitude represented something demonstrably better than what was available anywhere else at NIST and the resonance frequency would avoid some of the low-amplitude tonal vibrations present in the facility.

Development of Design. The prototype slab was designed to fit in an existing pit in a metrology laboratory space at NIST. This defined certain limits on the size and aspect ratios that could be employed. The existing pit was fairly deep, which gave the design team some flexibility in developing an appropriate cross-section to fit the fairly reasonable design criteria. To some extent, however, the development of the cross-section and the detailing of the spring supports were driven by practical requirements of constructability and the desire on NIST’s part to maximize opportunities to try different spring systems and layouts.

An additional feature of the concept was the use of what came to be called a “walk-on floor,” which was suspended above the isolated slab and supported by a separate load path. It would allow support equipment and personnel activities to be carried out without significant perturbation of the pneumatically isolated system, which would support only critical experimental equipment.

Finite Element Model. A finite element model (FEM) of the slab was constructed from 300 “solid” elements to represent the slab and 10 “beam” elements configured to simulate the axial and transverse stiffnesses of the airsprings. In addition, the concrete foundation beneath the slab was modeled using plate bending elements and the soil beneath the foundation was represented by massless spring elements. The entire FEM was implemented using GT-STRUDL®, a proprietary finite element software package operating on a Pentium desktop computer. The model was used to calculate resonance frequencies and modeshapes as well as to attempt development of a methodology that would allow users and/or designers to predict the vibration environment that would be provided by a given slab and airspring configuration using measured site vibration data.

Vibration Measurements. A measurement program was carried out that obtained the following data:

- Ambient vibrations in the pit and on the isolated slab with the airsprings inflated and deflated.
- Transfer functions from the pit to the top of the isolated slab.
- Vibration of the isolated slab due to walking on the walk-on raised floor system.
- Modeshape analysis of the airspring system and slab, with the intent of identifying natural frequencies and associated modeshapes.

Vibrations were measured using two sets of Mark model L-4 geophones as vibration sensors (nominal sensitivity of 0.18 v/ms^{-1}). One set was located in a void in the pit beneath the c.g. of the slab, and the other was moved from one location to another on the top of the slab. A Hewlett-Packard Model 35665A spectrum analyzer was used for data acquisition and processing. The slab resonance frequencies were identified using repetitive hammerblows with a rubber mallet. Once the resonance frequencies were identified, an Electro-Seis shaker was used to apply sinusoidal forces at each frequency while displacements relative to the shaker location were mapped.

3. DESCRIPTION OF SLAB CONSTRUCTION

The Inertia Slab. The plan dimensions of the slab were dictated by the dimensions of the existing pit, leaving adequate clearance along the sides and gaps at each end large enough for ladders to provide access. The airsprings and the bearing surface of the slab (when the airsprings were deflated) were beneath the slab. Preliminary sizing of the slab's thickness was by means of simple published relationships. These calculations suggested that a plate of a single thickness that would meet the resonance frequency criterion would pose certain constructability problems that might be reduced or avoided by the use of a keel, creating a T-shaped cross-section. In addition, the bottom of the keel could be used as a bearing surface to support the slab when the airsprings were deflated for maintenance. In its final configuration, the isolated slab had a T-shaped cross-section—a slab with a keel—as shown conceptually in Figure 1 and Figure 2.

The slab depth is 600 mm; the keel adds another 300 mm. The slab was constructed of normal weight concrete with a compressive strength of 28 MPa (4000 psi) using the minimum reinforcement specified by ACI. The weight of the slab was about 620 kN (140,000 lbs).

Pneumatic Support System. The isolated slab is supported on 10 commercially available airsprings rated to provide resonance frequencies of 1.5 Hz vertically and 3.1 Hz horizontally. Each spring has a rated capacity of 62 kN (14,000 lb). The airspring system was provided with a height control system that utilized noncontacting sensors (to avoid short-circuiting). This will be the extent of position control in the system for the time being, although provisions have been made to retrofit an active position control system (which was developed independently by NIST for another project) should the need arise. Eventually, the passive airspring system was supplemented by an active vibration control system to reduce amplification at the resonance frequencies of the mass on the airsprings, but the measurements were not repeated after that installation.

Walk-on Floor. The airspring-isolated slab is intended to support only vibration-sensitive apparatus; personnel and auxiliary experimental equipment are to be supported on an edge-supported “walk-on” floor. The top surface of the slab was placed about 400 mm below the elevation of the surrounding floor, which allowed the walk-on floor to be at the same elevation as the rest of the laboratory. The bearing surface of the walk-on floor was access floor tile supported on a framework of tubular steel that was supported from the edges of the pit.

It was determined after initial measurements of the system's performance that “ringing” of the relatively undamped steel framing of the walk-on floor was produced when people walked on the walk-on floor. This appeared on spectra measured on the isolated slab as several fairly narrow, tone-like vibrations that degraded the performance of the slab. This was resolved by installing neoprene vibration isolators at each location where the steel frame connected to the pit.

4. RESONANCE FREQUENCIES

Finite Element Model. The finite element model was used to calculate the resonance frequencies of the first 30 modes of the system. This set included 12 modes corresponding essentially to motion of the rigid mass on the airsprings and the foundation mass on the soil springs. The remaining 18 modes were associated predominantly with deformations of the slab. The first 8 of these modes had frequencies below 200 Hz, the limit of the range of interest for this study.

Hammerblow Response. A mallet was used to strike the slab at four locations, with exponentially averaged velocity response measured near the point of impact. The four locations included the center, one corner, and mid-length on each side. The test allowed for identification of most of the actual resonance frequencies. Figure 3

shows the velocity spectra measured at each location, from which spectra the resonance frequencies could be determined.

Comparison of Modeled and Measured Frequencies. The measured and calculated resonance frequencies are summarized in Table 1. Because of the slab’s nonsymmetric T-shaped cross-section, its deformations do not correspond to either “pure plate” or “pure beam” behavior. The labels **B₁**, **B₂**, and **B₃** were used to denote the first three modes similar to beam bending; **T₁**, **T₂**, and **T₃** to denote the first three modes similar to torsion of a prismatic section; **L₁** to denote the first combined flexural-torsional mode; and **R₁** to denote what might be called a “barrel” mode associated predominantly with bending about the longitudinal axis.

Table 1. Summary of Resonance Frequencies

Mode	Description	Frequency, Hz	
		Predicted	Measured
B₁	First bending mode	33	34
T₁	First torsional mode	39	52
B₂	Second bending mode	84	87
T₂	Second torsional mode	80	102
L₁	Lateral-torsional mode	91	112
B₃	Third bending mode	150	154
T₃	Third torsional mode	128	158
R₁	Barrel mode	174	-

Several observations may be made when comparing the two sets of frequencies:

- There is close agreement between the calculated and measured frequencies for modes **B₁**, **B₂** and **B₃**.
- The measured frequencies for modes **T₁**, **T₂** and **T₃** are 20 to 30 percent higher than those calculated using the FEM. No explanation was found.
- The ratios between measured frequencies of modes **B₁**, **B₂** and **B₃** are consistent with the corresponding published ratios for uniform free-free plates; the ratios between measured frequencies for modes **T₁**, **T₂** and **T₃** are approximately integers, more consistent with torsional vibration of a prismatic bar than with what would be expected with two-dimensional plate bending.
- The resonance frequency associated with mode **R₁** was not obtained in the hammerblow test, either because it could not be adequately excited or because its resonance frequency was above 200 Hz.

5. MODESHAPES

Finite Element Model. The finite element model was used to calculate the modeshapes of the first 30 modes of the system. Eighteen modes were associated predominantly with deformations of the slab. The first 8 of these modes had frequencies below 200 Hz, the limit of the range of interest for this study. The deformed shapes associated with these 8 modes are shown in Figure 4.

Measured Modeshapes using Forced Response. Review of the hammerblow data and the modeshapes produced by the FEM suggested antinode locations at which a dynamic force could be applied with an electrodynamic shaker to excite individual modeshapes. With the shaker producing a sinusoidal load at a frequency identified by the hammerblows, velocity magnitude and phase were measured relative to the motion at the point of excitation following a square grid pattern of approximately 600 mm. Magnitude and phase were combined in a spreadsheet

to determine relative amplitude. Contour maps and deformed shapes were produced using the software package SURFER®.

Comparison of Modeled and Measured Modeshapes. Despite the differences in measured *frequencies*, there appeared to be good correlation between *modeshapes* produced by the FEM and forced-response measurements. Figure 5, Figure 6, and Figure 7 show calculated (top) and measured (bottom) modeshapes and contour diagrams for four of the modes of interest. It was found quite difficult to obtain measurements with enough precision to locate the nodal lines accurately.

6. MEASURED PERFORMANCE - SPRINGS INFLATED

Ambient vibrations were measured at three locations (bottom of pit, center of slab, and one corner of the slab) with the airsprings inflated and deflated. In each location, the data were measured in three orthogonal directions. The data were processed in one-third-octave bands and in constant bandwidth. In addition, transfer functions were obtained for particular pairs of sensor locations and directions.

Triaxial Performance. Figure 8 shows the three directional components of ambient vibrations measured at the center of the isolated slab. The increasing amplitude as the frequency decreases toward 1 Hz is the result of the 1.4 Hz resonance frequency of the mass on the airsprings. The amplitude is greatest in the vertical direction, but the behavior is present in all three directions. On the other hand, the peaks in the 3.1 Hz band appear only in the horizontal directions; the nominal lateral resonance frequency of the airsprings is also 3.1 Hz. The vertical component exhibits a peak in the 31.5 Hz band, which is not present in the horizontal components. This is associated with the \mathbf{B}_1 mode, and a horizontal component would not be expected directly above the centroid of the mass.

Figure 9 shows the three directional components measured at one corner of the isolated slab. Here we see involvement of the vertical component in the 3.1 Hz peaks, suggesting that this motion involves rocking about both horizontal axes. We also see two peaks in the vertical curve between 10 and 100 Hz. The peak in the 31.5 Hz band is associated with the \mathbf{B}_1 mode; the peak in the 50 Hz band is associated with \mathbf{T}_1 mode. There is a peak in the E-W component (longitudinal direction) in the 31.5 Hz band and a peak in the N-S component (lateral direction) in the 50 Hz band; both of these suggest some coupling of horizontal motion with vertical at the corner.

At frequencies of 5 Hz and higher, the amplitudes in all directions are less than the criterion of 0.75 $\mu\text{m/s}$. At frequencies of 6.3 Hz and higher, the amplitudes are less than 0.2 $\mu\text{m/s}$, a significant reduction from ambient conditions available on-grade.

SRSS Performance. Because of the large quantity of data involved, the root-sum-square (SRSS) velocity amplitude—summing the three velocity directional components at one point—was used to simplify the presentation of measured data and assessment of isolation performance. In a manner of speaking, this represents the overall magnitude of the motion in each frequency band. Figure 10 shows the SRSS velocity amplitude measured at the bottom of the pit (below the airsprings) and at two locations on the slab surface.

As has been mentioned, the goal of the isolation system was to achieve a velocity of at most 0.75 $\mu\text{m/s}$ at frequencies above 8 Hz. The measured SRSS velocity obtained at frequencies above 5 Hz is about 0.2 $\mu\text{m/s}$, well below the goal. The performance in this frequency range is limited by the amplitudes in the 31.5 Hz and 50 Hz one-third octave bands. If these were reduced by about three-quarters in future designs, the achieved velocity would be on the order of 0.08 $\mu\text{m/s}$, almost an order of magnitude below the original goal.

Isolation System Performance. The peaks observed in the 31.5, 50 and 100 Hz one-third-octave bands are due to resonances of the slab. Figure 11 shows one measure of isolation system performance—the ratio between SRSS slab motion and SRSS base motion at the two measurement locations. It is evident that some degradation of isolation performance results from resonance amplification within the slab. The three peaks for which specific modes can be identified are marked. The reduced isolation at frequencies above 120 Hz is probably due to a combination of higher-order slab resonances and airspring nonlinearities.

7. MEASURED PERFORMANCE - SPRINGS DEFLATED

The airsprings suspend the slab above its support by only about 5 mm. The system was designed to allow deflation of the springs to facilitate their removal and/or relocation. Some of the users have expressed interest in using this feature in experiments where stability at very low frequencies is more important than isolation. When the springs are deflated, the spectrum of the vertical component is virtually identical to that of the base. The amplitude horizontal motion in the long direction was slightly higher on the slab than on the base at a wide range of frequencies between 16 and 40 Hz—indicating some degree of amplification (probably due to rocking) and fairly high damping—but the amplitude did not exceed 0.75 $\mu\text{m/s}$. In the short direction, the amplitude of the slab surface in the 25 Hz band was about 3 times that of the base, suggesting a great deal more rocking amplification (and thus lower damping) in this direction. This appears to be in general agreement with the frequency range predicted for foundation resonances in the FEM.

When the springs are deflated, the velocity amplitudes do not exceed the criterion for on-grade laboratory locations in the ATL.

8. DEFINING THE “SWEET SPOTS”

If the slab is excited by a blow, such as a dropped tool, it will respond by “ringing” at its resonance frequencies. (The hammerblow response in Figure 3 is an example of such response.) Upon reviewing the measured performance of the slab, it also became clear that some of the modes involving slab deformation contributed to a degradation of the isolation performance of the system as a whole. Thus, it became desirable to identify the locations on the slab at which these effects would be minimized (which the users dubbed the “sweet spots”). To some extent, this was as simple as identifying the nodal lines—the lines along which there is no translation of the slab—but the location of individual nodal lines is a function of frequency.

Figure 12 shows the calculated contour diagrams for modes \mathbf{B}_1 , \mathbf{T}_1 , and \mathbf{T}_2 , with the nodal lines approximated with solid heavy lines. The two dots mark the “sweet spots,” locations that have no vertical translation at any of these resonance frequencies. It is important to note, however, that there will be rotation at these locations, so a test object that extends up from the slab in cantilever fashion will experience *horizontal* motion at these frequencies.

9. PREDICTABILITY OF PERFORMANCE

It was desired to examine the feasibility of using FEM to predict motions of the isolated slab on the basis of motions measured below the airsprings. The most straightforward means of assessing this capability appeared to

be through the use of transfer functions. These were produced using the FEM to calculate the response of the slab to a fictitious dynamic loading of the base. A unit load was applied at the bottom of each spring. The loads at all ten points of application were in phase. (This was done for the sake of simplicity. A preliminary study showed that response of the system in the frequency range of concern was relatively insensitive to phase relationships, probably because of the compliance of the isolation system. Since the true excitation is random ground motion with random phase relationships between the ten supports, the alternative of using a more simplified analysis was quite attractive.)

Figure 13 shows the vibration velocity response curves resulting from application of a vertical force of 1 newton to the foundation below each airspring. Three curves are shown: (1) vertical base (foundation) motion, (2) vertical motion at the center of the inertia slab, and (3) vertical motion at one corner of the inertia slab. The resonance peaks have been marked, along with peaks associated with response to foundation resonances (identified with an "F"). At very low frequencies (below 0.5 Hz) the isolators are effectively rigid, as one would expect from theory, and the motion of the base and the slab are of the same amplitude. At approximately 1.5 Hz, the system's vertical resonance frequency—based on the slab mass and the isolator stiffness—is manifested as an amplification of the slab velocity relative to the foundation velocity. Above this frequency the slab's velocity drops relative to the foundation velocity (because the inertia force of the mass is much greater than the spring force), thereby showing the typical and expected vibration isolation increase with increasing frequency. Up to about 15 Hz the slab effectively behaves as a rigid plate on springs. Above 15 Hz, the foundation and the slab start to exhibit structural resonances manifested by peaks at about 23 and 51 Hz and at higher frequencies.

Figure 14 shows the calculated ratio of the slab's vertical response to vertical base vibration. It shows this "transfer function" ratio for the two points on the top of the inertia slab discussed previously. Portions of the curve above a value of 1 indicate amplification, and those below indicate attenuation. The heavy line represents the transfer function between the base and the center of the slab, and the lighter line between the base and the corner. The corner-to-base transfer function shows a resonance at about 52 Hz, which corresponds with the T_1 mode of the slab; this peak is not as pronounced at the center location because this modeshape's nodal lines pass through the center of the slab. The resonance peak seen at 34 Hz corresponds with the B_1 mode, which can be seen in both the center- and corner-to-base transfer functions.

The fine line in Figure 15 shows a measured FFT transfer function relating vertical motion of the center of the slab to that in the pit below the slab; the heavier line shows the same transfer function calculated from the FEM. At frequencies below 50 Hz, there is a general similarity of shape, but at frequencies greater than 50 Hz there is very little similarity.

It should be noted that comparison in this manner considers only transfer functions in *parallel* directions; the effects of coupling will be neglected. However, the measured velocity spectra of the three components of base motion are quite similar (see Figure 8 and Figure 9). Close comparison of the coupling transfer functions with the parallel transfer functions suggests that vertical motion of the slab is a function of *all three* components of base motion. Figure 16 shows the transfer functions defining vertical motion of the center of the slab surface resulting from all three components of base motion. Between 3 and 20 Hz, the vertical base motion provides the predominant definition of the slab motion, but at higher frequencies the distinction isn't as clear. Figure 17 shows the corresponding transfer functions defining vertical motion of one corner. At some frequencies the horizontal base motion components contribute more to vertical movement than does vertical base motion. Clearly, since the amplitude of the horizontal base motion is similar to that of the vertical, it must not be neglected.

We can make the simplifying assumption that the three components of base motion are equal and in phase, then combine the three transfer function components (base vertical to slab vertical; base N-S to slab vertical; base E-W to slab vertical) using SRSS methodology. This can be carried out for both for the center and the corner of the

slab surface. This will produce the transfer functions shown in Figure 18. Comparison of the two curves suggests that for a given ambient base motion, the vertical amplitudes at the corner will significantly exceed those at the center for almost all frequencies. That was indeed observed in the measurements.

Bearing in mind the slight differences between measured and calculated resonance frequencies, the two transfer functions in the previous figure were compared with the measured transfer function relating vertical slab motion to vertical base motion.

At many frequencies below 120 Hz, the transfer function measured at the center of the slab bore a good similarity to the curve calculated for the corner and the center. (The similarity of the measured center transfer function to the calculated *corner* transfer function suggests that the use of in-phase loading—which implies symmetry—may be too simplified to accurately model the real situation.)

Assuming that the *actual* response of the slab is more "smeared" than the finite element would predict, we calculated the geometric mean of the transfer functions for the center and corner. Figure 19 shows this geometric mean transfer function compared with the measured one. The curves are fairly similar. Some of the differences are due to offsets between measured and calculated resonance frequencies; some others are due to differences between assumed and apparent damping at resonances.

Despite the similarity between the measured and calculated data at frequencies below about 120 Hz, the model does not adequately predict the increased response above 120 Hz. (The behavior above 120 Hz is most likely due at least in part to deviation of the airsprings' behavior from that of an ideal linear massless spring or from disturbances that reach the slab through paths that do not involve the airsprings.) It appears that the motion of the system is subject to variables that cannot be adequately defined so that accurate finite element modeling of slab response to a realistic ground-motion input cannot be accomplished.

Unfortunately, a scheme to resolve the significant differences between measured and calculated *horizontal* transfer functions does not suggest itself. It is possible that the difference is real.

10. CONCLUSIONS

This study documented the dynamic characteristics and vibration isolation performance of one of the largest isolation masses ever built for use in a laboratory environment. It also identified the extent to which finite element modeling could be used to predict behavior of a pneumatically supported system. The primary findings are summarized below.

- Finite element analysis (FEA) of the type used here can predict natural frequencies and mode shapes fairly well, but it does not predict bending and twisting modes with equal accuracy. Some improvement might be possible with a finer element mesh.
- FEA is inadequate for the prediction of response of an isolated slab to ground vibrations. The vibration measured on the slab in a given direction may be due to flexure and rotational motions of the spring supports and the springs themselves. (This was demonstrated by the complex combination of base components to achieve a single vertical transfer function.) A finite element model would not be able to represent this behavior.
- Significant nonlinearities may occur in the springs at the small amplitudes with which we are dealing, so that pit motion at one frequency may give rise to motions at a multitude of frequencies. This may apply more to horizontal motion of the slab.

- Mass-airspring resonances can cause an order of magnitude or more amplification at the airspring resonance frequencies.
- Deviation of airspring behavior from that of an ideal massless spring may cause a significant degradation in isolation performance at frequencies above 100 Hz, perhaps by as much as two orders of magnitude.
- Slab resonances degrade isolation performance, perhaps by as much as an order of magnitude. These must be considered during design, and perhaps mitigated either by sizing the slab to achieve resonances above the frequency range of interest or by designing increased damping into the slab structure.

ACKNOWLEDGMENTS

This research project required the involvement of many individuals. The authors wish to express their gratitude the National Institute of Standards and Technology for its generous support and to the following people: Stephen J. Lind, Carol Parssinen, Louis R. Quartararo and Eric E. Ungar at Acentech Incorporated; Charles B. Randolph and Chi Nguyen at Henningson Durham & Richardson, Inc.; Chris Conley and K. C. Patel at NIST; Peter Roy and David Talley at CRSS; and Rodney Horning at Barry Controls. A special debt is owed to Samuel Kramer, former Deputy Director of NIST, for his unflagging support of this effort to develop a better understanding of the vibration isolation of large laboratory spaces.

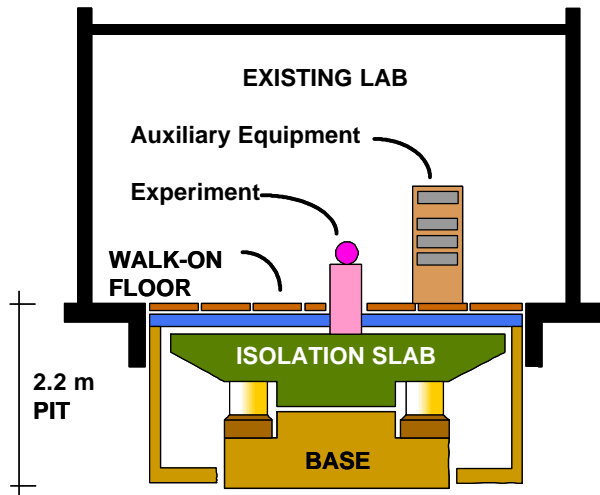


Figure 1. Cross-section of lab and isolation slab show how the airsprings support the concrete slab, while the walk-on floor rests on the walls of the pit. (Drawing courtesy HDR, Inc.)

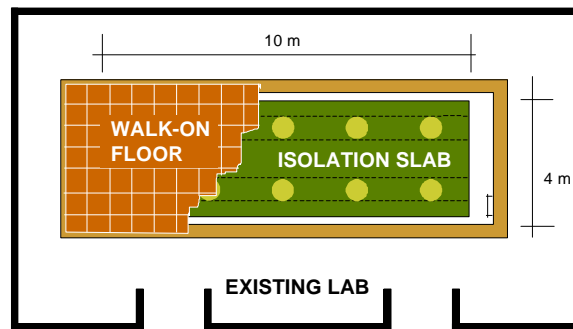


Figure 2. Plan view of lab and isolation slab with a portion of the walk-on floor cut away. (Drawing courtesy HDR, Inc.)

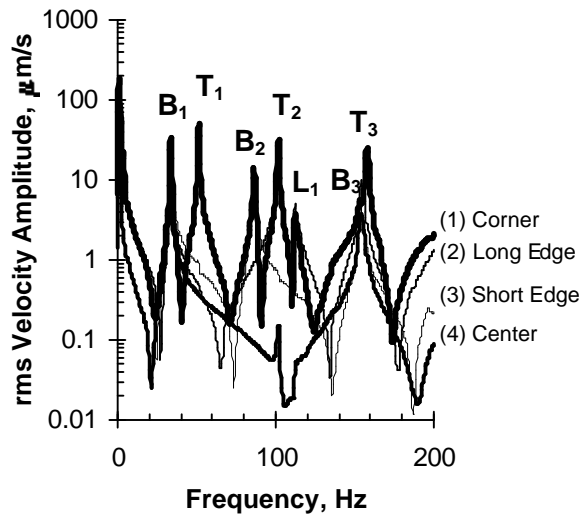


Figure 3. Velocity spectra due to hammerblows, measured at four locations on the slab.

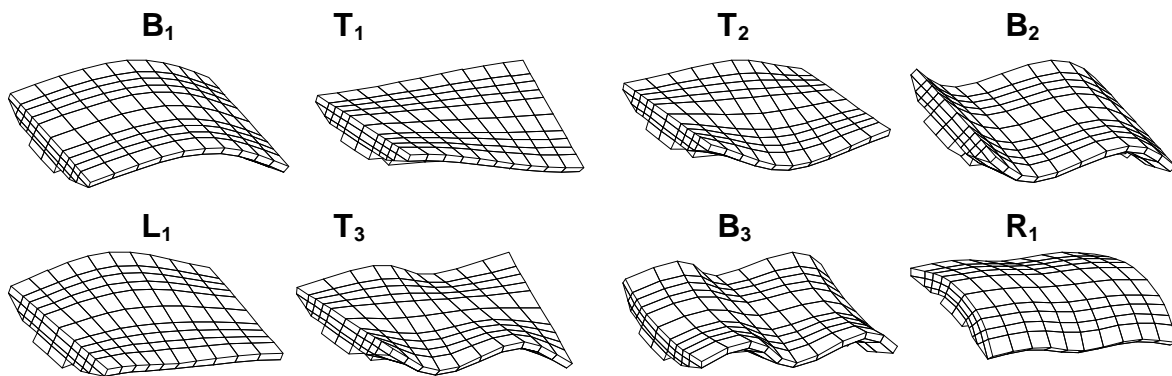


Figure 4. Deformed shapes associated with structural resonances with calculated frequencies less than 200 Hz.

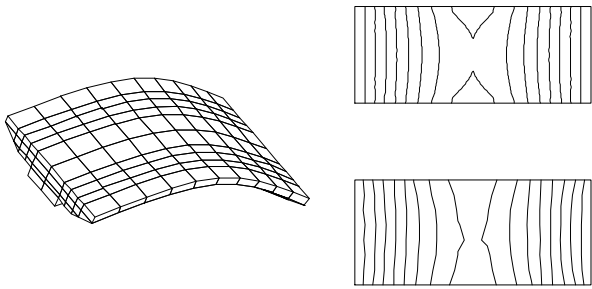


Figure 5. Computed deformed shape (left), computed contour diagram (top right) and measured contour diagram (bottom right) for mode \mathbf{B}_1 .

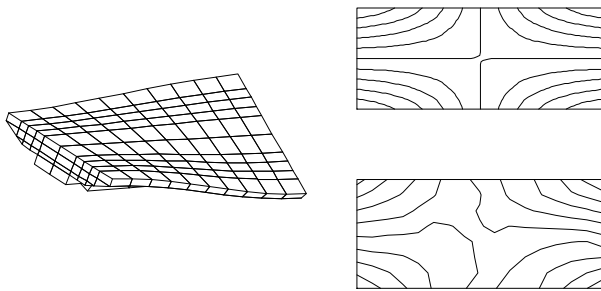


Figure 6. Computed deformed shape (left), computed contour diagram (top right) and measured contour diagram (bottom right) for mode \mathbf{T}_1 .

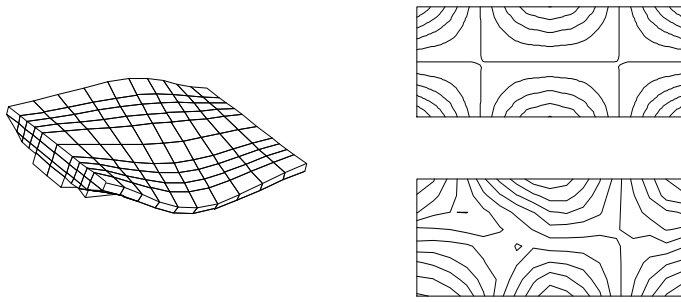


Figure 7. Computed deformed shape (left), computed contour diagram (top right) and measured contour diagram (bottom right) for mode T_2 .

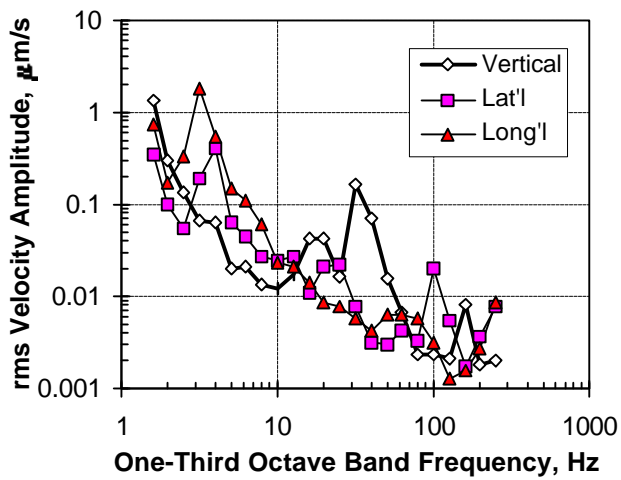


Figure 8. Triaxial representation of ambient vibrations measured at center of isolated slab.

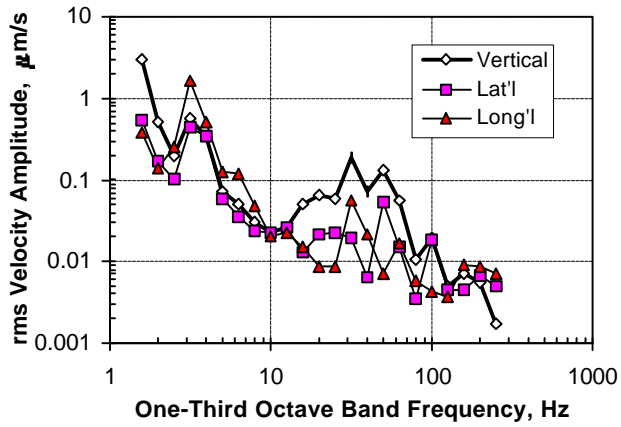


Figure 9. Triaxial representation of ambient vibrations measured at one corner of isolated slab.

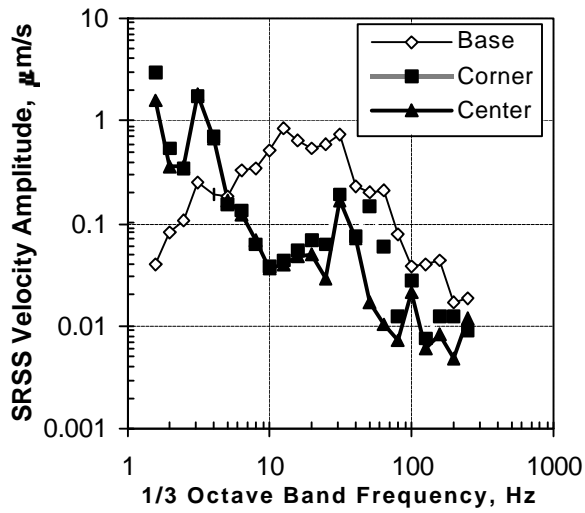


Figure 10. SRSS representation of ambient vibrations in the pit at the center and corner of the slab.

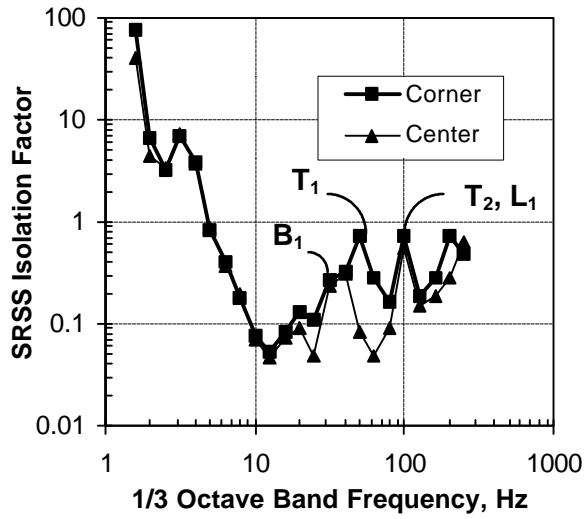


Figure 11. SRSS representation of isolation system performance at the center and corner of the slab.

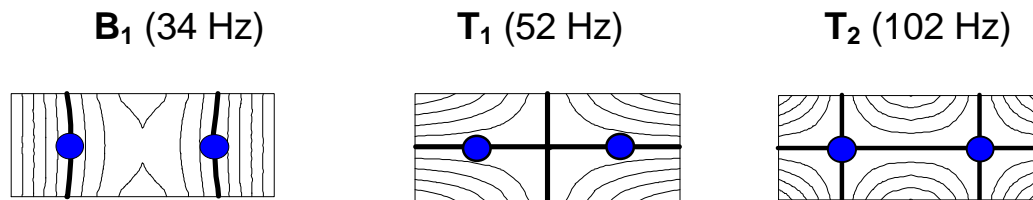


Figure 12. Calculated contour diagrams for modes B_1 , T_1 , and T_2 , with approximate nodal lines. Dots mark the "sweet spots" for the combined effects of these three modes.

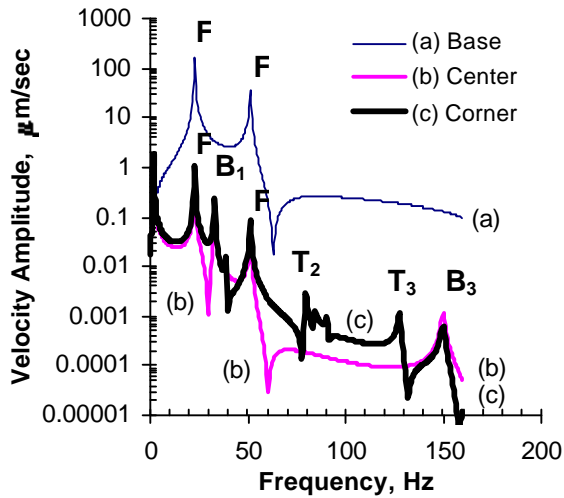


Figure 13. Calculated vertical velocity response due to simultaneous in-phase application of a 1 newton vertical force beneath each airspring. Shown are curves for (a) foundation motion, (b) center of the isolated slab, and (c) corner of the isolated slab.

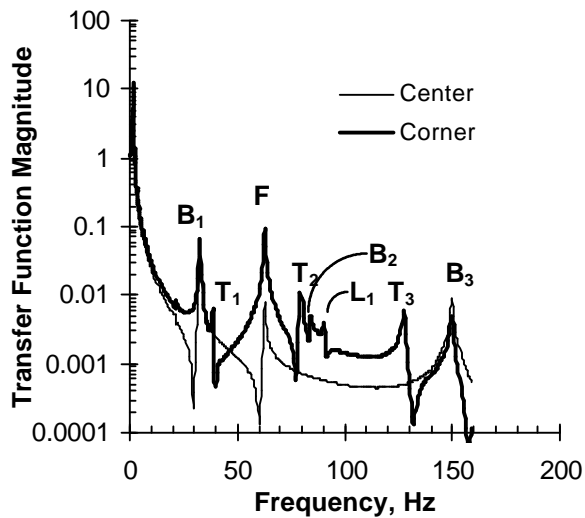


Figure 14. Calculated ratio (transfer function) between slab's vertical response (at the center and corner of the slab) and the vertical base excitation.

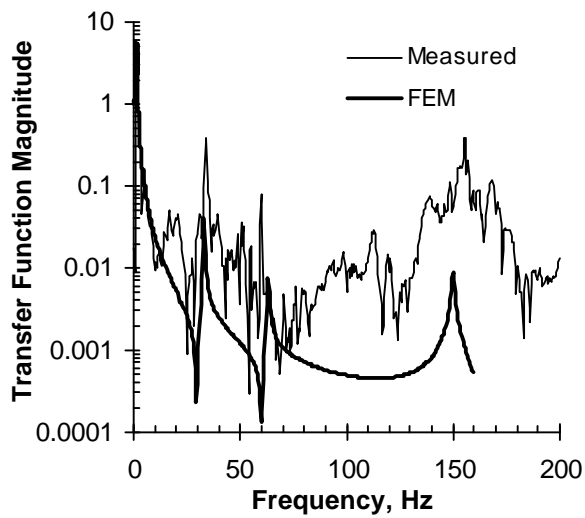


Figure 15. Measured FFT transfer function between velocity measured at the bottom of the pit ant that measured at the center of the slab.

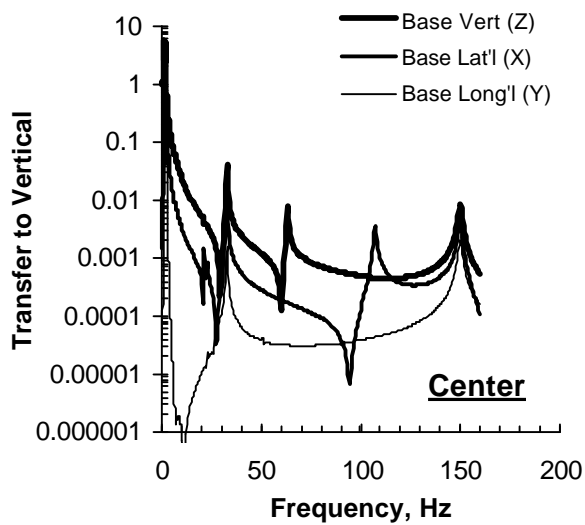


Figure 16. Calculated transfer functions defining vertical motion of the center of the slab resulting from each of three components of base motion.

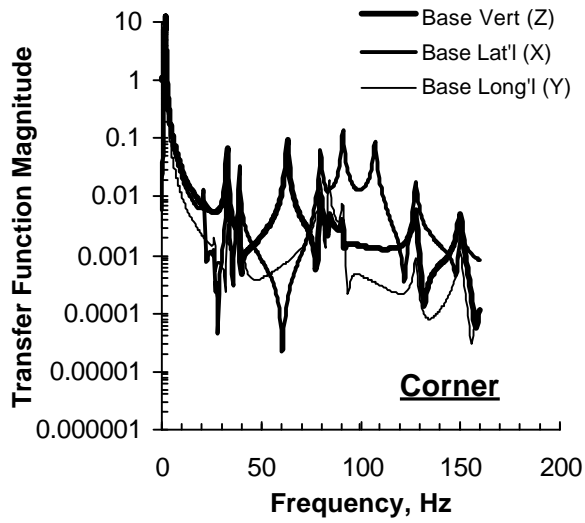


Figure 17. Calculated transfer functions defining vertical motion of the corner of the slab resulting from each of three components of base motion.

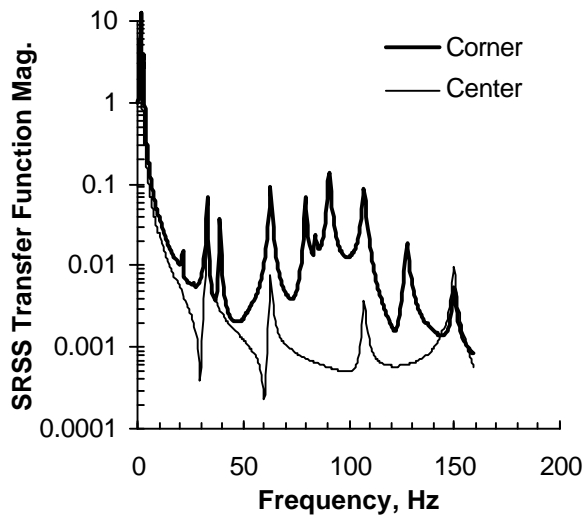


Figure 18. Calculated SRSS transfer functions defining vertical motion of the center and corner of the slab as combination of three components of base motion.

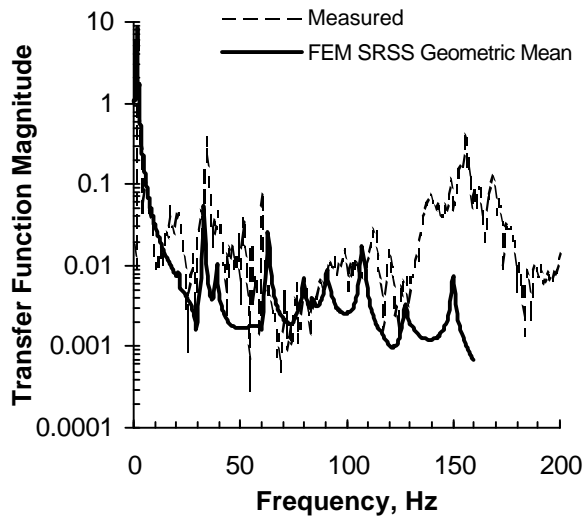


Figure 19. Comparison of the calculated "geometric mean" transfer function with the measured transfer function.